doi:10.26443/seismica.v4i2.1688

Retrieval of body waves with seismic interferometry of vehicle traffic: A case study from upstate New York, USA

Diego A. Quiros *[1], **Larry D. Brown**[2]

[1]Department of Geological Sciences, University of Cape Town, Cape Town, South Africa, 7701, [2]Department of Earth and Atmospheric Sciences, Cornell University, Ithaca, New York, USA

Author contributions: *Conceptualization*: D. Quiros, L. Brown. *Data Curation*: D. Quiros. *Formal Analysis*: D. Quiros, L. Brown. *Investigation*: D. Quiros, L. Brown. *Methodology*: D. Quiros, L. Brown. *Writing – original draft*: D. Quiros. *Writing – review & editing*: D. Quiros, L. Brown.

Abstract Seismic interferometry of vehicle traffic recorded by a vertical seismograph array along a highway in upstate New York has recovered surface and body waves that match the velocities of waves in the Devonian and Silurian shales. Faster arrivals extracted via interferometry align with P-waves from a controlled-source refraction survey and with local velocities derived from seismicity in the study region, while the slower linear arrivals agree with Rayleigh waves observed in the refraction survey. Traffic volume shows significant variation between peak and non-peak hours. Amplitude variation is minimal, reducing the need for normalization to extract body waves; nonetheless, better results are obtained when cross-coherence is used in conjunction with small time windows to reduce crosstalk among the vehicle sources, given their transient nature. In comparison to other seismic sources such as trains, vehicle traffic also has a broadband signature, although more compact in time as shown by spectrograms. The results presented here suggest that vehicle traffic can function as an effective seismic source for body wave interferometry under the right conditions and survey geometries.

Production Editor: Yen Joe Tan
Handling Editor: György Hetényi
Copy & Layout Editor: Hannah F. Mark

Received: April 6, 2025
Accepted: September 11, 2025
Published: October 15, 2025

Resumen (Español) La interferometría sísmica del tráfico vehicular en una carretera de Nueva York recuperó ondas superficiales y de cuerpo con velocidades que coinciden con las lutitas devónicas y silúricas de la región. Las llegadas rápidas se alinean con las ondas P de un estudio de refracción, mientras que las llegadas más lentas corresponden a ondas de Rayleigh. Aunque el tráfico se observó constantemente, hay un contraste significativo entre las horas pico y de bajo tránsito. La variación de amplitud es mínima, lo que reduce la necesidad de normalización para extraer ondas de cuerpo; sin embargo, se logran mejores resultados con coherencia cruzada y ventanas de tiempo pequeñas para minimizar la contaminación entre fuentes vehiculares. En comparación con otras fuentes sísmicas, el tráfico vehicular presenta un espectro de banda ancha pero más compacto. Los resultados sugieren que el tráfico puede ser una fuente sísmica efectiva para la interferometría de ondas de cuerpo bajo las condiciones adecuadas.

Non-technical summary Researchers studied vehicle traffic along a highway in upstate New York using a specialized equipment setup and advanced techniques to analyze the vibrations created by the vehicles. They found that the waves produced matched well with the characteristics of certain underground rock formations, found from more standard techniques. The amount of traffic varied significantly between busy and quiet times. Interestingly, the variations in the strength of the signals were not large, making it easier to analyze the data without significant adjustments. However, using specific techniques helped improve the quality of the results by equalizing the strength of the signals. Overall, the study suggests that vehicle traffic can be a useful source for gathering seismic data, which could help in understanding the underground structures, when the right conditions are met.

1 Introduction

In the past two decades seismic interferometry (SI) has become an important tool in the seismological toolkit. The origins of SI can be traced to the work of Claerbout (1968) and later to the developments in the early 2000's by Bakulin and Calvert (2004), Schuster et al. (2004), Snieder (2004), Wapenaar (2003, 2004), and Wapenaar and Fokkema (2006). Fundamentally, SI is used to estimate the acoustic or elastic Green's function between two locations. The retrieved seismic trace corresponds to the recording by one receiver of a virtual excitation at the location of the other (Wapenaar et al., 2004). Early examples focused on recovering the surface wave Green's function from cross-correlation of simultaneous seismic records (e.g., Shapiro et al., 2005), as the seismic field is known to be dominated by fundamental mode surface waves below frequencies of 0.1 Hz (Ekström, 2001; Haubrich et al., 1963; Toksöz and Lacoss, 1968). Subsequent work was also aimed at the extraction of body waves from the seismic field (Roux et al.,

*Corresponding author: diego.quiros@uct.ac.za

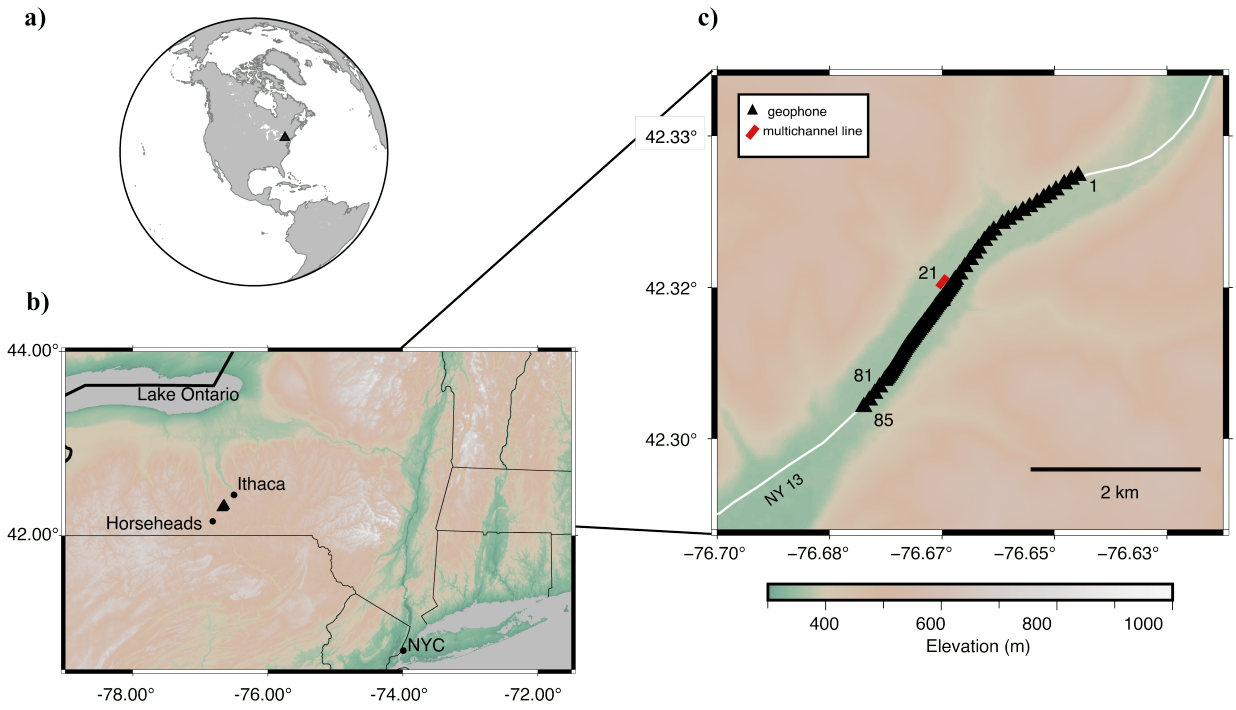

Figure 1 a) Global map centered in North America with location of experiment shown by black triangle. b) Regional map of upstate New York showing location of survey (black triangle). c) Station map showing seismographs as black triangles, a multichannel refraction survey as red line and NY13 highway as a white line. Notice the location of the survey within a glacial valley.

2005; Ruigrok et al., 2010; Ryberg, 2011; Draganov et al., 2008).

Although most of the work in SI has been directed towards the seismic field generated by natural processes, the anthropogenic component of the field has become an important source for SI studies. Early SI examples using anthropogenic sources include structural imaging of a tunnel using vehicle sources (Matsuoka et al., 2006; Shiraishi et al., 2006), surface wave retrieval from vehicle traffic (Halliday et al., 2008), and measurements of shear-wave splitting from recordings by a borehole array of mechanical noise at the surface (Miyazawa et al., 2008). More recent work has explored railroads (e.g., Brenguier et al., 2019; Quiros et al., 2016), urban traffic (e.g., Nakata et al., 2015, 2011), mining activity (e.g., Chamarczuk et al., 2022), and even wind farms (e.g., Spangler and Nowack, 2022) as sources for interferometric imaging. Of these sources, vehicle traffic due to cars and trucks in suburban and urban environments is the most abundant, and unlike traditional controlled sources, vehicle traffic represents no cost to the surveyor, is relatively stable over time, has minimal environmental effects, and can be considered wideband (Liu et al., 2021).

Several studies have applied SI to vehicle traffic with varying degrees of success. In general, these can be further divided into those focused on the retrieval of surface waves (e.g., Behm and Snieder, 2013; Mi et al., 2022) and those focused on the retrieval of body waves (e.g., Nakata et al., 2015, 2011). In this study we apply inter-receiver SI to a vehicle traffic dataset collected along a highly transited stretch of road between the urban centers of Ithaca and Horseheads in upstate New York, with the goal of retrieving body waves and to better characterize vehicle traffic as a source for interferometry.

2 Deployment

In the fall of 2011 eighty-five vertical component seismographs were deployed along New York State Route 13 (NY 13) within a glacial valley, 16 km southwest of Ithaca, NY (Figure 1). The equipment was obtained from the SAGE instrument pool (previously IRIS-PASSCAL) of the Earthscope Consortium.

The experiment itself was a spinoff of the larger Virginia AIDA 2011 project (e.g., Brown et al., 2011, 2012) which focused on recording the aftershock sequence of the 5.8 Mw Mineral Virginia earthquake, but which also recorded large volumes of vehicle traffic along a complex network of local roads. The numerous local roads in Mineral, Virginia presented added complexity to understand vehicle traffic as a seismic source, thus the decision was made to re-deploy some of these instruments under simpler experimental conditions.

The site near Ithaca, NY was chosen for several reasons: (1) the road geometry is relatively straight, (2) it lies within a glacial valley far away from other roads and additional sources of anthropogenic noise, and (3) it has a large traffic volume between the urban centers of Ithaca and Horseheads, NY.

For the NY 13 experiment each seismograph consisted of a Ref Tek 125A recorder (i.e., Texan) and a 4.5 Hz vertical component geophone (Geospace GS-11D). Data acquisition was continuous from 23 September till 4 October 2011 (i.e., 265 hours). Each station was buried approximately 30 cm below the surface. The linear ar-

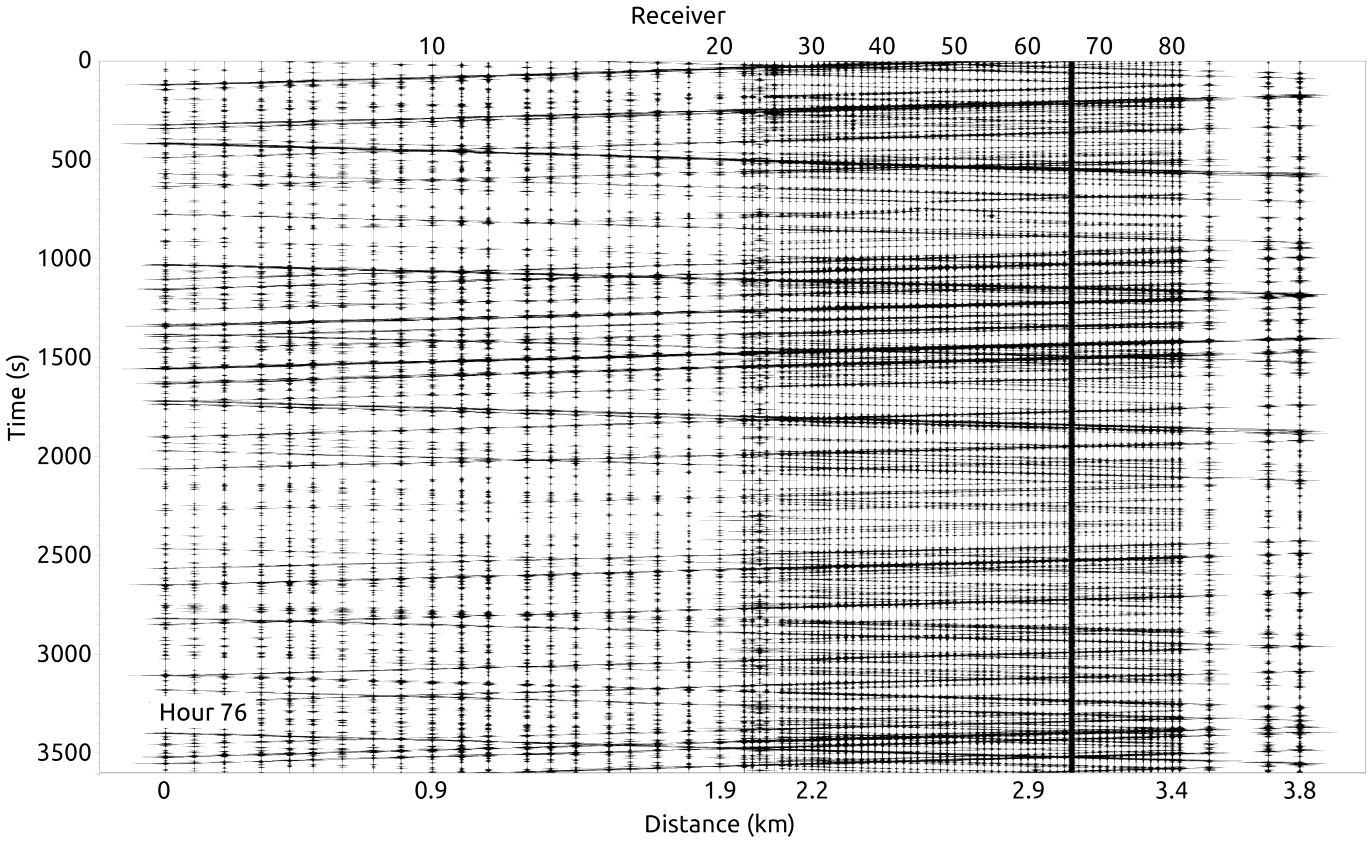

Figure 2 Raw seismograms of the 76th hour of recording. Events dipping to the right correspond to vehicles traveling from NE (i.e., station 1) to SW (i.e., station 85), while events dipping to the left correspond to travel in the opposite direction. The horizontal axis corresponds to the distance from station 1. Note that station 66 recorded high frequency noise. The largest amplitude dipping events likely correspond to semi-trucks (lorries) traveling through the array while the smaller amplitude dipping events correspond to passenger vehicles.

ray was deployed from NE to SW (Figure 1b) over a three-day period with the help of graduate students who volunteered. On day one stations 1 – 25 were installed, while on day three stations 26 – 85 were installed. Simultaneous recording of all 85 stations took place for a period of 172 hours (i.e., 7.16 days).

The array used two inter-station spacings, an inner segment of sixty-one stations were spaced 25 m apart (i.e., stations 21 – 81), bracketed between flanking segments with spacing of 100 m. The length of the array was approximately 3.9 km. To maintain each Texan continuously recording each datalogger needed its D-cell batteries replaced every 3 days as their original design was for controlled-source seismology. The sampling rate used was 100 Hz corresponding to a Nyquist frequency of 50 Hz.

A separate controlled-source seismic refraction experiment was completed on 15 January 2014 using a shotgun source and a 48-channel seismograph with vertical component geophones spaced every 3.05 m (Figure 1c) to constrain the subsurface seismic velocities. This survey was collected between receiver locations 21 and 26 (i.e., beginning of the denser section of the main Texan deployment, shown with a red line on Figure 1c).

3 Data

The continuous data was acquired in hour-long windows (or gathers). Subsequently the data was filtered to remove the non-zero mean value (DC component) of the waveforms inherent in the Texan recorders. Inspection of the raw data shows several dipping events which correspond to vehicular traffic along NY 13 (Figure 2).

Although vehicle traffic was observed during every hour of data, during the hours of the early morning, 1 – 3 a.m. local time (i.e., 5 – 7 UTC time) the volume of traffic considerably diminishes, although no hour-long record is free of vehicular traffic. Figure 3 shows a comparison of night and day traffic along NY 13 for the hours 1 a.m. and 4 p.m. local time of 27 September 2011.

The nighttime record in Figure 3a presents the lowest volume of traffic found in the data (i.e., quietest period), while the daytime record in Figure 3c shows peak volume of traffic. Both records are normalized by the combined peak value amplitude (i.e., ensemble normalization) for easier comparison. Another approach is to compare the average amplitude spectrum of each hour-long record: Figure 3b shows the spectrum for the nighttime record (lowest volume of traffic observed), while Figure 3d shows the spectrum for the daytime record (peak volume of traffic observed). These spectra effectively represent the lower (Figure 3b) and upper (Figure 3d) amplitude limits found in the data, although

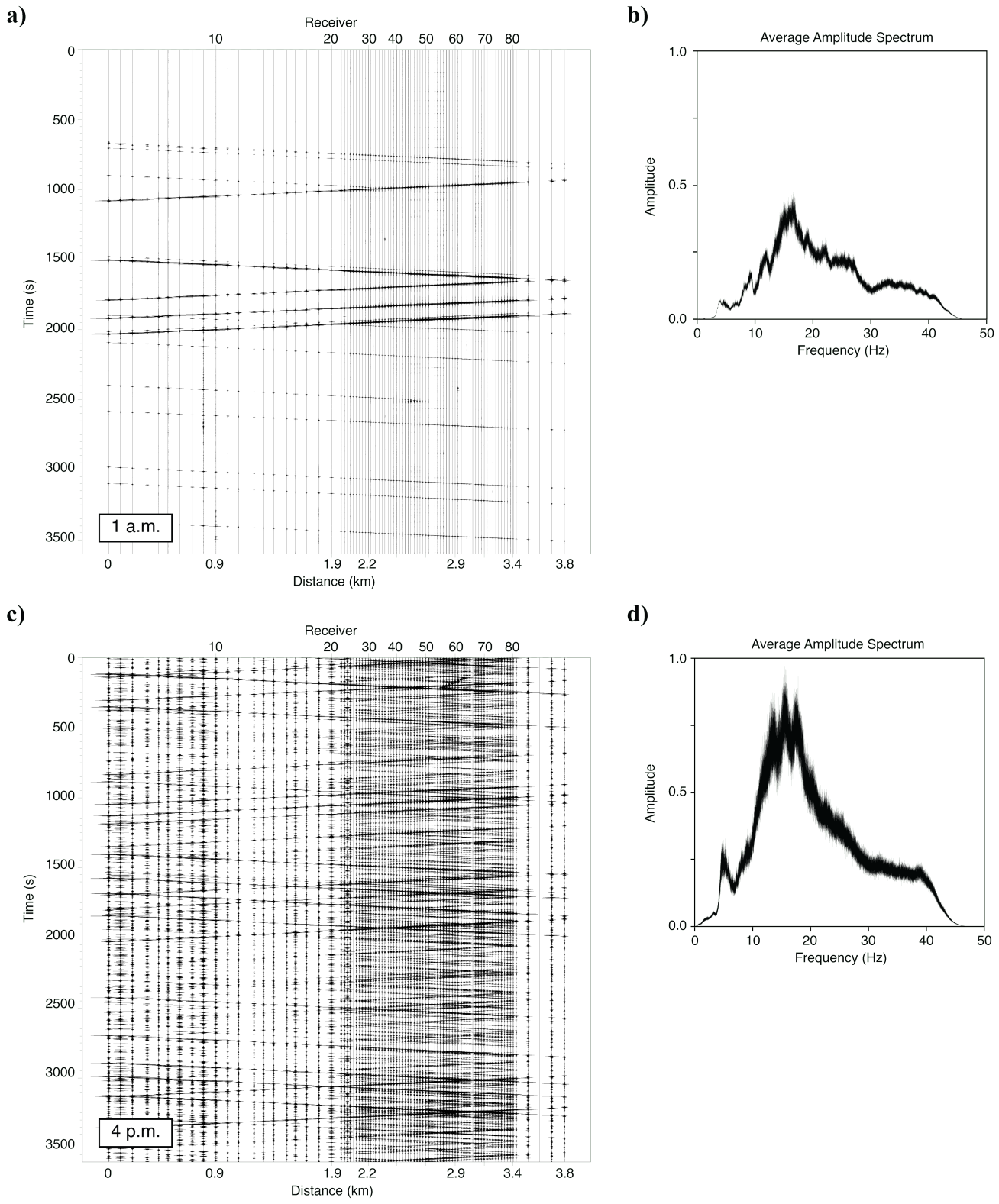

Figure 3 Example of vehicular traffic volume during night and day periods. a) Hour-long recording starting at 1 a.m. local time (hour 89 of recording), for 27 September 2011. This hour-long record presents the lowest volume of traffic found in the dataset. Larger amplitude events between 1500 and 2000 s are likely semi-trailer trucks. b) The average amplitude spectrum derived from a). c) Hour-long recording starting at 4 p.m. local time (hour 104 of recording), for 27 September 2011. This hour-long record represent peak traffic hours. d) The average amplitude spectrum derived from c). Records a) and c) are normalized by the combined peak value amplitude.

most of the dataset has average amplitude spectra closer to Figure 3d, which is simply the result of having considerably less hour-long records with low traffic volumes.

The spectral character of vehicular seismic signatures was investigated by examining multiple stations. As an example we select one station (i.e., station 17) on three different hour-long data windows and extract three different vehicular seismograms. Note that simi-

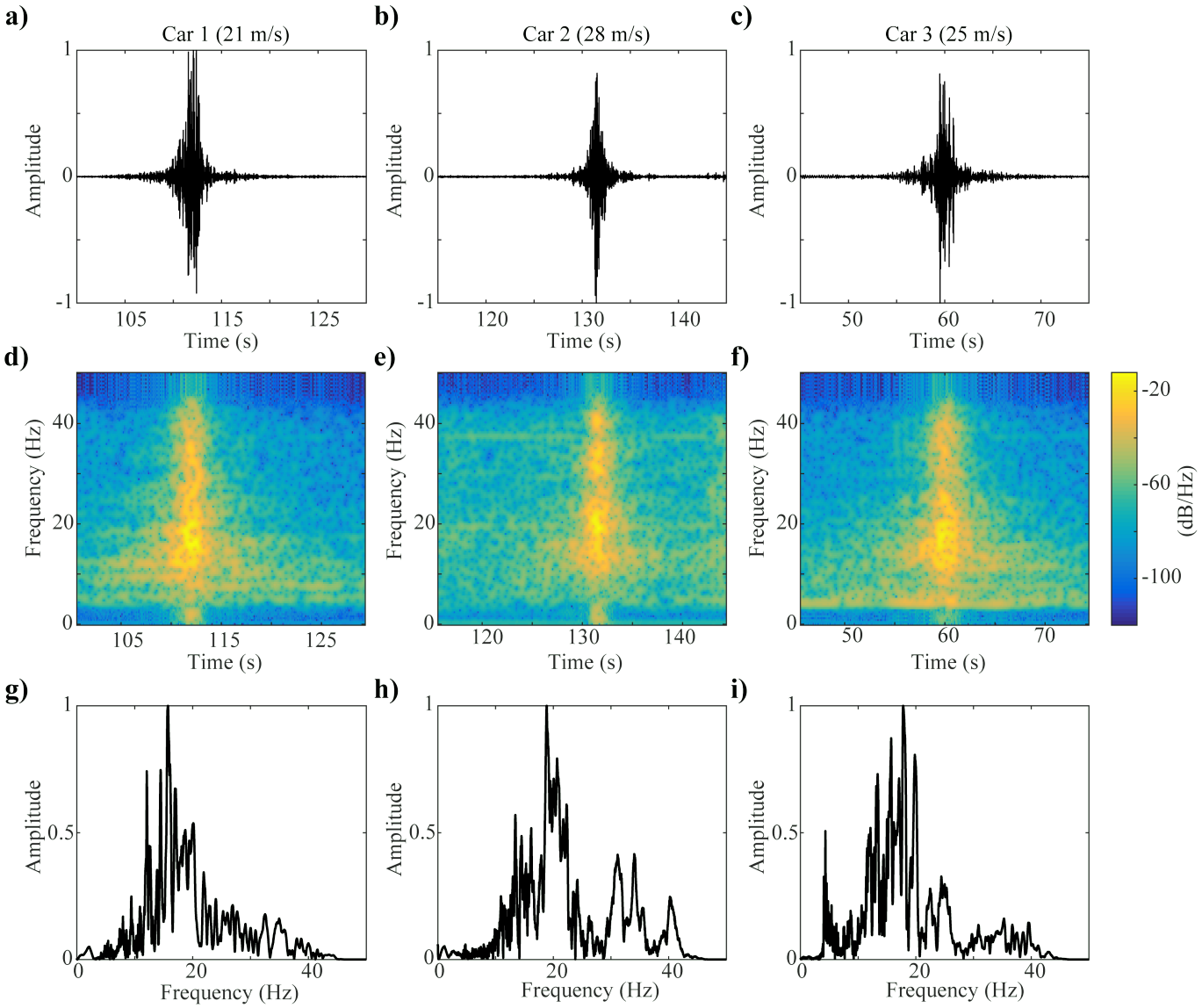

Figure 4 Frequency analysis of vehicle traffic. Top row a) – c) shows seismograms for station 17 extracted from three different hour recordings. All traces are individually normalized to their peak amplitude (i.e., trace normalization). Middle row d) – f) shows the corresponding spectrograms. Bottom row g) – i) shows the corresponding amplitude spectrum.

lar spectral behavior was observed across the array and there is nothing special about the selected station. The top row in Figure 4 shows three seismic traces which correspond to station 17 extracted from different hours. The middle row shows spectrograms of these seismic traces, and the bottom row shows their amplitude spectrum. The speed shown in Figure 4a – c was obtained by measuring the slope of a dipping event (i.e., the speed of a vehicle passing through the array) on each data gather before extracting the trace for station 17. The spectrograms show very similar behavior across the different traces examined, with high frequencies (f_H > 20 Hz) only visible when the vehicle is very close to the station, and much lower frequencies when the vehicles are approaching and fading from the station. Finally, the amplitude spectra show a broadband signal for all example traces, with energy peaking just below 20 Hz. Not surprisingly, these spectral characteristics agree with previous reports in the literature (e.g., Meng et al., 2021; Riahi and Gerstoft, 2015).

4 Methods

To generate interferometric source gathers, several preprocessing routines were tested. In the simplest case no temporal normalization was applied prior to interferometric processing. The reasoning behind this was that the amplitudes of vehicle traffic are similar from hour to hour in the dataset, as shown by the amplitude bounds in Figures 3b & 3d. Other normalization routines tested were spectrum balancing (i.e., whitening) and one-bit normalization.

The initial interferometric processing was done via cross-correlation of receiver pairs, where a station is selected and cross-correlated with all others in each hour-long data gather. Following this, amplitude normalization is applied on a trace-by-trace basis within each cross-correlation gather or panel, and then all panels are normalized to equalize the amplitudes between different panels (ensemble normalization), and finally all panels are summed (stacked) to generate an interferometric gather with 85 traces. This procedure is repeated

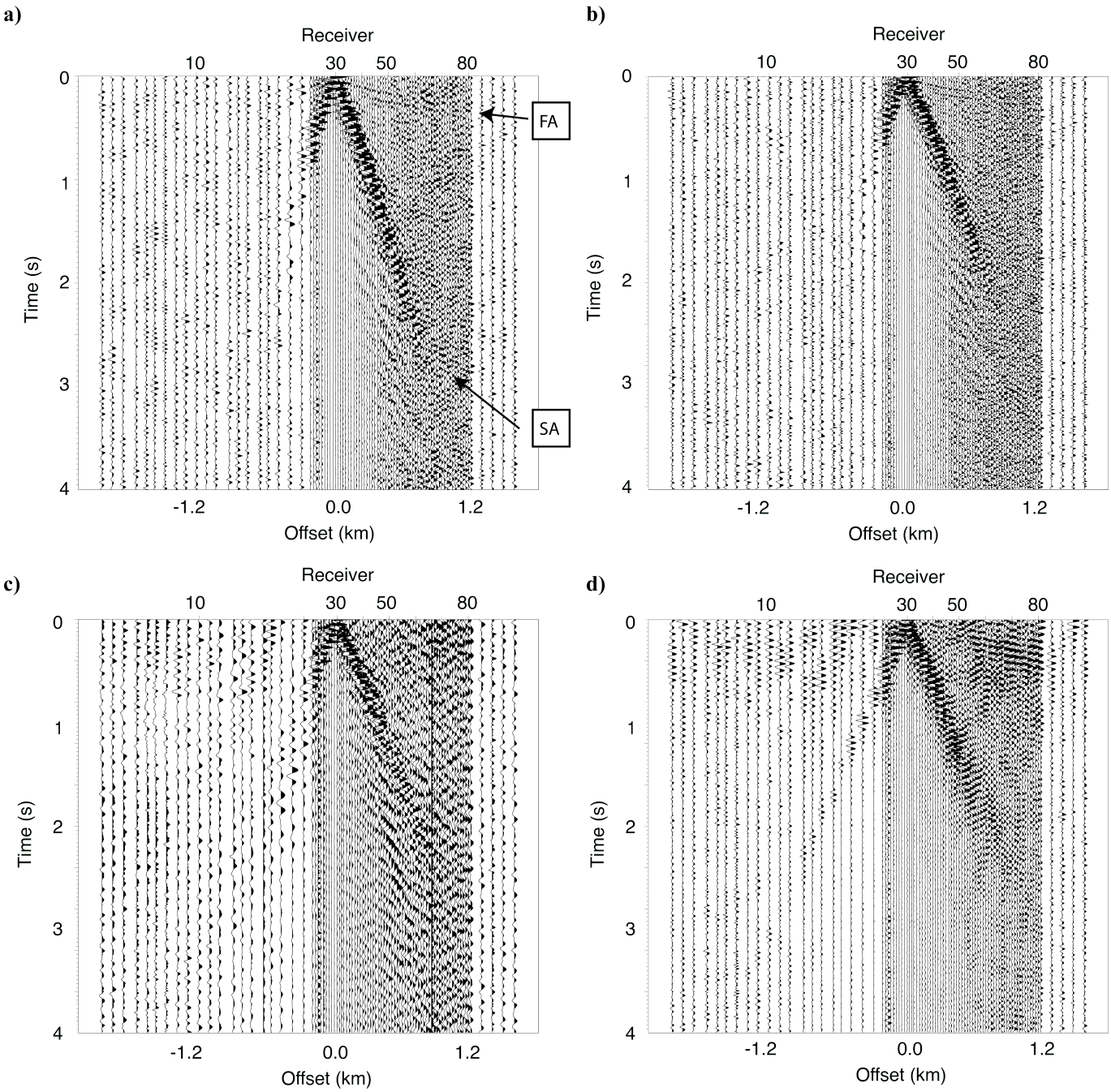

Figure 5 Positive lags of the virtual source gather generated by cross-correlation interferometry, amplitude normalization and stacking with various preprocessing sequences. a) No amplitude normalization prior to processing, and no filter applied for display, where the faster arrivals discussed in the text are indicated by FA and the slower arrivals by SA. b) Spectral balancing (whitening) prior to processing, and no filter applied for display. c) One-bit normalization prior to processing, and no filter applied for display. d) One-bit normalization prior to processing, and a bandpass filter (10 – 48 Hz) is applied for display. All panels are displayed with individual trace normalization to enhance faster arrivals.

for all stations, resulting in 85 interferometric gathers (one for each station).

Figure 5 shows the results obtained with the different preprocessing routines using hour-long data windows and the interferometric processing described in the previous paragraph for station 29 as the virtual source. Panels a) – c) do not include any filtering while panel d) has been filtered between 10 – 48 Hz during preprocessing. All panels show large amplitude arrivals propagating from the location of station 29 with speeds between 280 – 410 m/s, which are likely Rayleigh waves exhibiting little dispersion. Weaker arrivals are also visible on all panels (i.e., top 0.5 s) with a speed of approximately 4800 m/s.

To test the effect of increased stacking on the interferometric gathers, we divided each 1-hour long data window into 200 s, 60 s, and 10 s windows, which results in 18, 60, and 360 data windows, respectively, for every hour of data. The reasoning behind using smaller data windows is that the vehicles traversing the array are transient sources, and not uncorrelated noise sources producing a diffuse wavefield (Wapenaar and

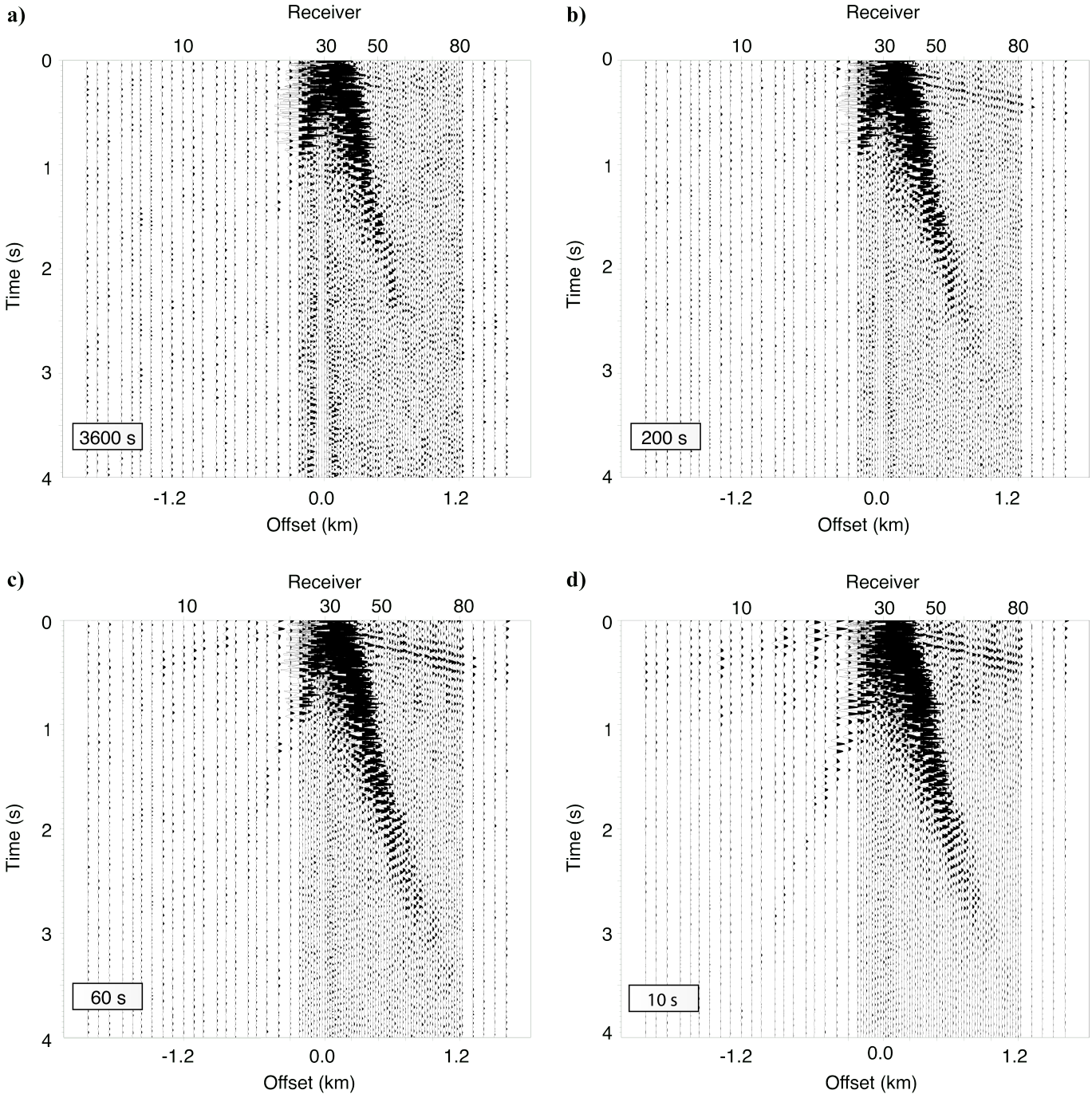

Figure 6 Effect of data window size on the coherency of arrivals. No amplitude normalization is done prior to the cross-correlation as amplitude variability across the dataset is low. a) Data window size is 1 hour. b) Data window size is 200 s. c) Data window size is 60 s. d) Data window size is 10 s. Records are normalized by the combined RMS value (i.e., ensemble normalization).

Fokkema, 2006; Draganov et al., 2008). It is well established that the length of the correlation windows should not matter if dealing with a diffuse wavefield; however, for the application of SI with transient sources, each source must be measured independently (Wapenaar and Fokkema, 2006). This means that using shorter correlation windows reduces the probability that two or more sources will fall on the same data window introducing artifacts (e.g., crosstalk between sources) in the cross-correlation gathers. The results of this comparison are shown in Figure 6, and as one would expect for SI with transient sources such as vehicles, the smaller data windows (e.g., 60 and 10 s) result in increased coherence for both the fast and slow arrivals described earlier.

In addition to standard cross-correlation, cross-coherence interferometry (i.e., power-normalized cross-correlation) is tested as it has been reported by some authors (Nakata et al., 2015, 2011; Barman et al., 2023) to enhance the coherency of arrivals retrieved in the virtual source gathers. To test the effectiveness of cross-coherence versus cross-correlation the data is divided into 10 s windows, guided by the results shown in Figure 6d. For the interferometric processing,

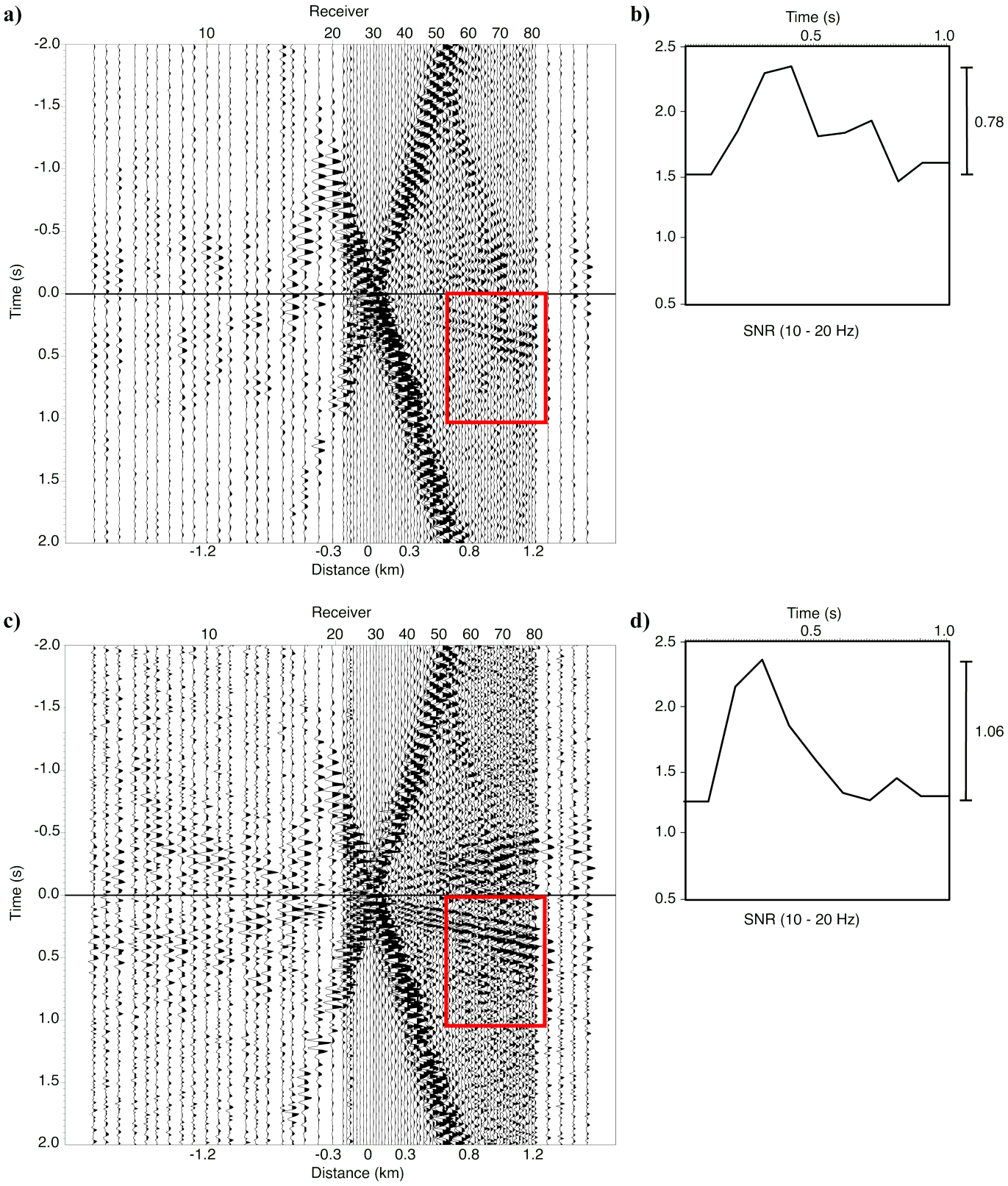

Figure 7 a) Positive and negative lags of the virtual source gather for station 29 for standard cross-correlation. Red box indicates SNR analysis window. b) SNR as a function of time for the frequency band 10 – 20 Hz. Bar on the right indicates SNR level relative to the start of the seismic window where there are no arrivals. c) Positive and negative lags of the virtual source gather for station 29 for cross-coherence. Individual trace scaling is applied to compare both gathers and to increased signal coherence for faster arrivals. d) SNR as a function of time for the frequency band 10 – 20 Hz. Bar on the right indicates SNR level relative to the start of the seismic window where there are no arrivals.

cross-correlation and cross-coherence are applied to each window and then all the generated gathers are normalized before stacking. The results are shown in Figure 7, where the virtual source gather obtained via cross-correlation (Figure 7a) and cross-coherence (Figure 7c) are displayed with both negative and positive

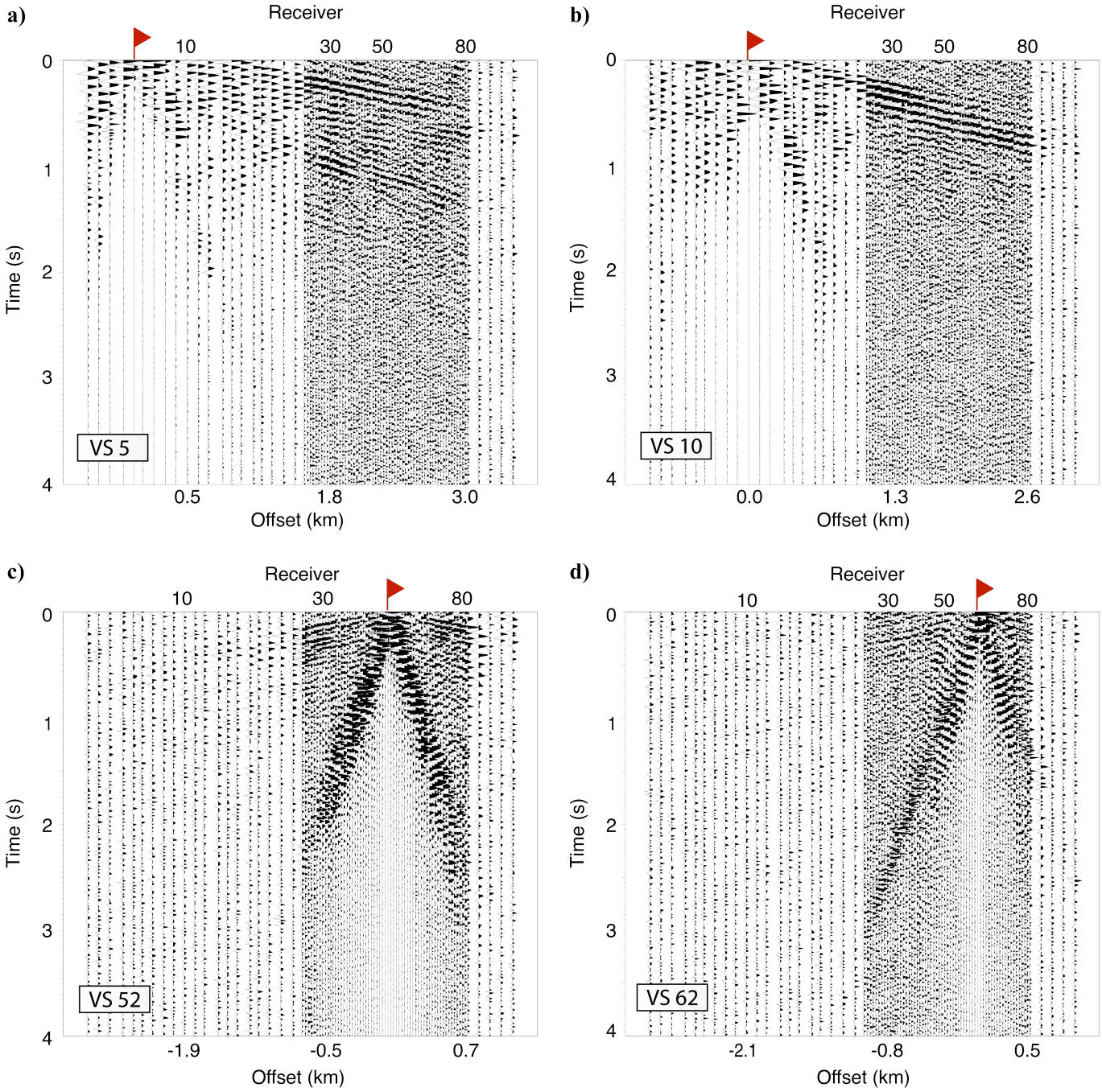

Figure 8 Positive lags of virtual source gather derived from cross-coherence interferometry. a) Virtual source at receiver 5 near the NE end of the array. b) Virtual source at receiver 10. c) Virtual source at receiver 52. d) Virtual source at receiver 62. Red flag indicates virtual source position.

lags (unlike previous examples). Results are filtered above 10 Hz to enhance the high-frequency faster arrivals. Improvement can be seen in the retrieval of these arrivals, especially at shorter offsets with cross-coherence. To quantify this improvement the signal-to-noise ratio (SNR) is computed within the windows (red box) shown in Figures 7a & 7c, where each trace is assumed to contain signal and uncorrelated noise. Using

$$SNR = \frac{1}{\sqrt{\frac{|A|}{|C|} - 1}}$$

one can estimate the level of signal relative to uncorrelated noise between two seismograms, where A is the zero-lag value of the autocorrelation of the first trace, and C is the maximum value of the cross-correlation of the two traces (e.g., Holbrook et al., 2013). The calculation is done with small subsets of data within the window, each subset is 200 ms by four seismic traces, with an overlap of 50%. Averaging SNR across the time axis produces the plots in Figures 7b & 7d, for the frequency band 10 – 20 Hz. The results of the SNR estimation show that the cross-coherence interferometry produces higher SNR results for this dataset, as indicated by the vertical bar (Figures 7b & 7d) with value 0.78 and 1.06 for cross-correlation and cross-coherence, respectively. Previous work by Nakata et al. (2011) demonstrates that cross-coherence produces higher SNR results com-

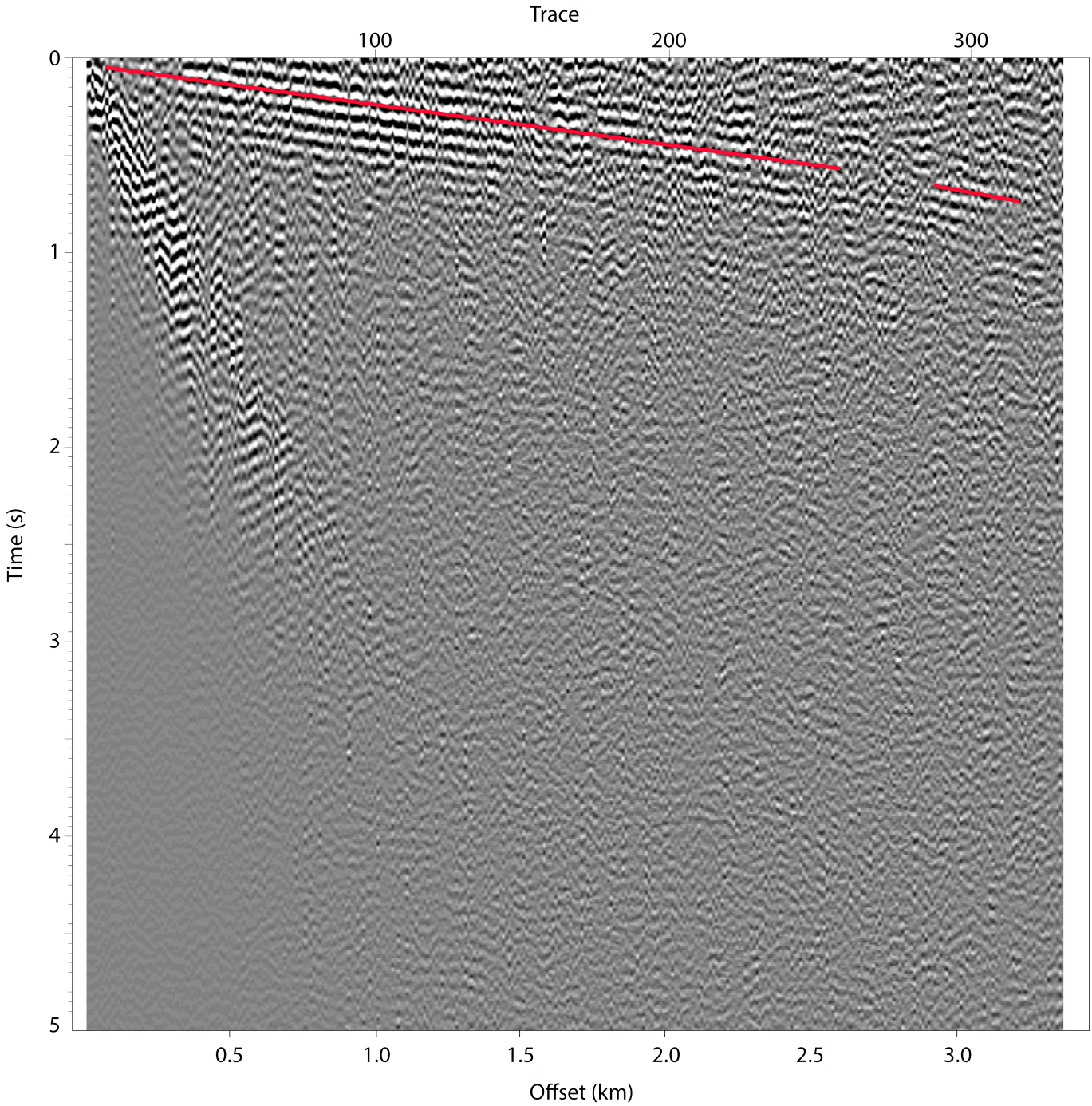

Figure 9 Common-offset stack virtual gather generated over all virtual source gathers with a 10 m bin size. The long red line which is picked through the zero-crossing of the faster arrival emanating from the source indicates a velocity of ~ 5070 m/s.

pared to methodologies like cross-correlation and deconvolution interferometry, especially when large amplitude variations are present in the data. Although this is not the case for the NY 13 dataset (e.g., Figure 3), we still observe an improvement from cross-coherence relative to cross-correlation interferometry.

Using other stations as the virtual source to generate interferometric gathers shows similar arrivals to those observed in Figures 5 – 7. Nonetheless, not all receiver locations appear to work well as virtual sources. For example, Figure 8 shows the virtual source gather obtained via cross-coherence for four different receiver locations. Figure 8a shows the virtual source gather generated at receiver location 5 (i.e., VS 5). Here, faster arrivals appear to emerge from receiver 13 instead of 5, as would be expected. These of course are spurious arrivals that are likely related to the bend in the geometry of the array near station 13, and/or to crosstalk between multiple sources. It should be noted that this bend in the array geometry which follows the trace of NY 13 likely results in traffic traveling between stations 14 – 85 to act as sources in non-stationary phase locations for stations 1 – 13, and vice versa. While Figure 8b generated at receiver location 10 appears more in-line with previous observations of these faster arrivals with apparent velocities of 4800 m/s, it still suffers from spu-

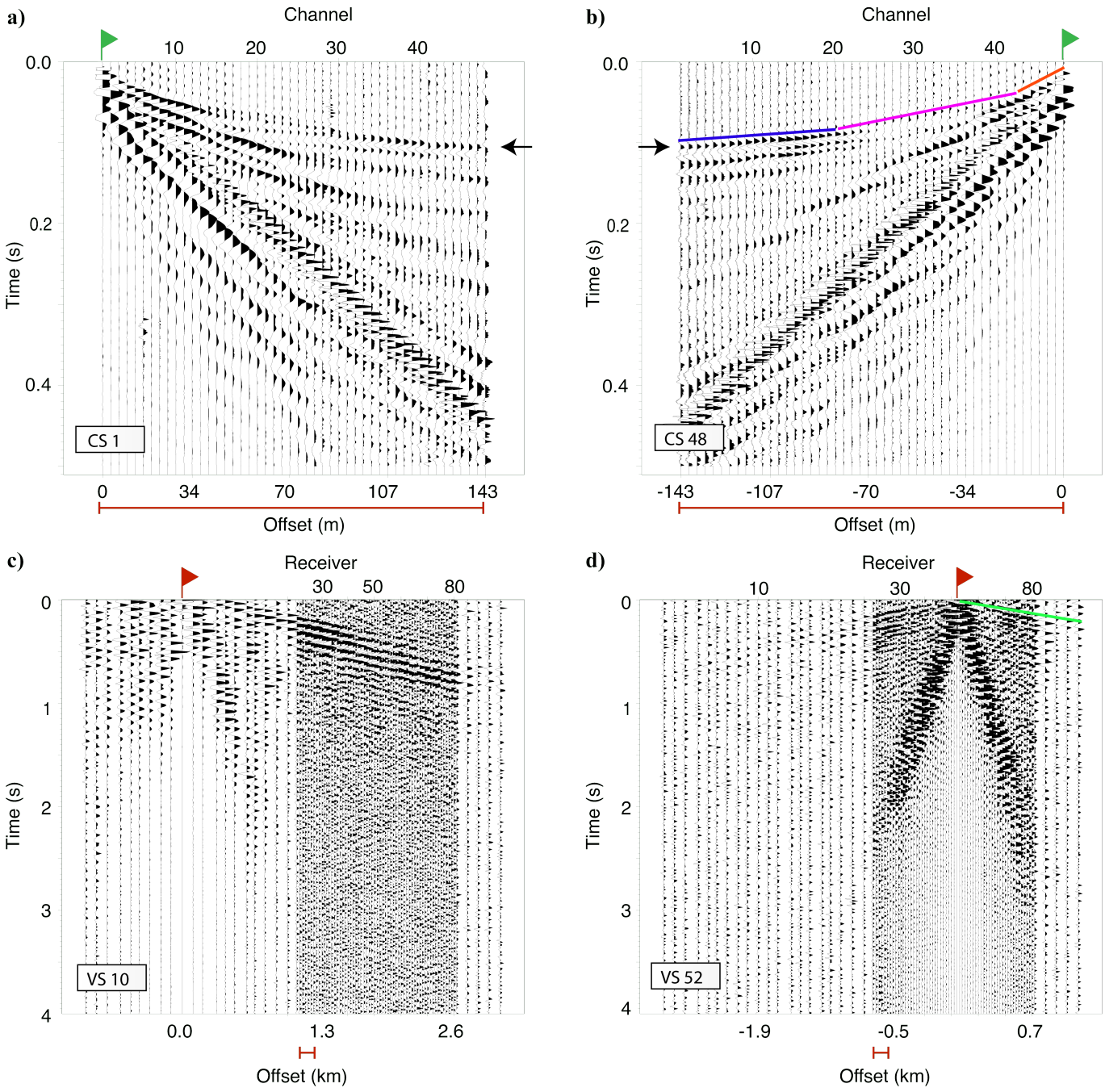

Figure 10 Controlled source shot gathers versus virtual source gathers. a) Controlled-source shot gather recorded by 48-channel seismograph. Channel spacing is 3.05 m, with channel 1 placed roughly at the location of receiver 21 of the Texan array (see Figure 1b). Green flag indicates the location of shotgun source. The red line below the offset axis indicates aperture of multichannel array. Black arrow indicates the direct arrival. b) Controlled-source shot gather with source at channel 48. Black arrow indicates the direct arrival, red line corresponds to a velocity of ~ 600 m/s (|offset|< 30 m), magenta line to a velocity of ~ 1600 m/s, and blue line to a velocity of ~ 3600 m/s (|offset|> 115 m). c) Virtual source gather at receiver 10. Red flag indicates the location of the virtual source. The red line below offset axis indicates aperture of multichannel array relative to the Texan array. d) Virtual source gather at receiver 52. The green line corresponds to a velocity of ~ 4800 m/s.

rious arrivals that emerge from station 13, again likely associated with the bend in the geometry of the array. Figure 8c shows the faster arrivals we have come to expect, emerging from the location of the virtual source at receiver 52. While a virtual source 225 m away (Figure 8d) shows that the coherence of the faster arrivals decreases substantially.

Finally, to try to better observe the faster arrivals over a wider aperture, a common-offset stacked virtual gather was generated (Figure 9). This offset gather is created by sorting the traces within all virtual source gathers into common-offset bins of 10 m and stacking them using a simple normalization of 1/(N+1), where N is the number of traces in each bin. In the common-offset stack the faster arrivals are visible to offsets of over 3 km with almost complete continuity. The red line on Figure 9 follows the zero-crossing of the faster arrival, its speed is measured to be approximate 5070 m/s,

which is higher than previously approximated from single virtual source gathers.

5 Discussion

Up to this point we have shown, as others have done (Behm and Snieder, 2013; Nakata et al., 2011; Behm et al., 2013), that vehicle traffic can be a rich source for seismic interferometry. Our results indicate that virtual source gathers obtained via different preprocessing methodologies (e.g., Figure 5) and different interferometric approaches (e.g., Figures 7 and 8) retrieve a variety of seismic arrivals with different velocities.

To characterize the arrivals retrieved by SI we use the small multichannel controlled source line described in the deployment section (Figure 1c). Figure 10 shows a comparison between the controlled-source survey and virtual source gathers obtained with SI. The reader should be aware that the multichannel survey has a small aperture (i.e., maximum offset 143 m) compared to the Texan array (i.e., maximum offset 3800 m), and this is indicated in Figure 10 a – d by the extent of the red lines below the offset axes.

The velocities observed for the direct arrival in the controlled-source shot gathers (Figures 10a and 10b) change with offset which is indicative of subsurface stratification (i.e., layering) or, in the continuous case, a velocity gradient. Since the channel spacing is only 3.05 m, it is reasonable to assume that the velocities observed at short offsets (|offset| < 30 m) in Figures 10a and 10b corresponds to direct P-waves travelling in the soil or unconsolidated layer (v_p ~ 600 m/s), while at large offsets (|offset|> 115 m) the direct arrivals represent a diving P-wave traveling in more consolidated material or sedimentary rocks (v_p ~ 3600 m/s). Refraction analysis of the controlled-source gathers based on these velocities and intercept times for the second (t_1 = 29.25 ms) and third layer (t_2 = 59.75 ms) shown in Figure 10b results in thicknesses of 9.5 and 25.5 m for a total depth to the fast velocity material of approximately 35 m. Considering that the critical and cross-over distance for a critical refraction from the deeper interface is approximately 30 m and 75 m, respectively, it would be extremely unlikely to observe any direct arrivals from the shallow layers on the Texan array data given the interstation spacing used (i.e., 25 m for the denser section). On the other hand, the faster arrivals extracted from the SI approach have velocities on the order of 4800 m/s (Figures 10c and 10d) and are observed at considerably larger offsets due to the aperture of the Texan array. Comparing of velocities of the faster arrivals retrieved via SI and those obtained at the larger offsets in the multi-channel survey (vp 3600 m/s at |offset|> 115 m), suggests that the SI processing is retrieving body waves from the traffic noise. Furthermore, a seismic velocity model obtained from natural local seismicity near the city of Ithaca, NY (Suhey et al., 2021) confirms P-wave velocities of 4.9, 5.4, and 5.9 km/s at depths of 1, 1.5 and 3 km, respectively, which is in good agreement with the velocities retrieved from SI of approximately 4.8 – 5.0 km/s (Figures 9 and 10). These velocities correspond to the Devonian and Silurian shales of the Appalachian Basin sector of New York state, which are penetrated by more than 100 boreholes within an area of 65 km^2 (Tamulonis et al., 2011) that includes this study.

Lastly, it is important to mention that the virtual sources derived via SI show no clear evidence of arrivals with hyperbolic moveout (i.e., reflections) which limits our ability to attempt any type of seismic reflection imaging. Additionally, the surface waves extracted via SI (e.g., Figures 5 & 6) show very little dispersion, suggesting a fairly homogeneous velocity structure once below the unconsolidated layer.

6 Conclusions

In this study we retrieve P-waves generated by vehicle traffic via seismic interferometry as recorded by a local dense linear array in upstate New York. The velocities obtained for the P-waves match those of Devonian and Silurian shales in upstate New York. The extraction of body waves is accomplished via different preprocessing methodologies and via different interferometric approaches as well. Due to the similar ground motion amplitudes generated by the vehicle traffic over time simple normalization routines appear sufficient prior to interferometric processing, while cross-coherence appears superior to standard cross-correlation when examining the coherency of the retrieved virtual source gathers. Interestingly, a bend in the geometry of the array appear to generate virtual sources with spurious arrivals, suggesting that perhaps processing arrays with multiple bends in straight segments might partially alleviate this issue in the future.

The results presented here and from previous studies suggest that vehicle traffic can function as an effective seismic source under the right conditions and survey geometries.

Acknowledgements

The authors wish to thank Noël Barstow, Steve Azevedo, and Pnina Miller from EARTHSCOPE-EPIC (formerly IRIS-PASSCAL) for technical guidance with instrument programming and data downloading. We also thank Chen Chen, Patrick Mulcahy, Philip Lee, William Barnhart, Mary Kosloski, Anastasija Cabolova for helping with the deployment, maintenance, and recovery of Texan stations, and Doyeon Kim for assisting in the multichannel refraction survey. D. Quiros received funding from the Earth and Atmospheric Sciences Department at Cornell University during the time of data collection. The authors thank editor Prof. György Hetényi and two reviewers for valuable comments that improved the manuscript. We also thank Prof. Deyan Draganov for insightful comments on early results.

Data and code availability

The raw seismic Texan data in SEGY format is available through the University of Cape Town open data institutional repository (ZivaHub) (Quiros, 2025b), as is the station metadata in a csv file (Quiros, 2025a). The software

Vista3D provided by SLB (i.e., Schlumberger) via academic licensing is used for data handling, processing, and most figures containing seismic data, while PyGMT (Tian et al., 2025) was used to create Figure 1, and Obspy (The ObsPy Development Team, 2024) was used to create Figure 4.

Competing interests

The authors have no competing interests.

References

Bakulin, A. and Calvert, R. Virtual source: new method for imaging and 4D below complex overburden. In *SEG Technical Program Expanded Abstracts 2004*. Society of Exploration Geophysicists, Jan. 2004. doi: 10.1190/1.1845233.

Barman, D., Pulliam, J., and Quiros, D. A. Ambient seismic noise tomography of the Suwannee suture zone using cross-coherence interferometry and double beamforming. *Geophysical Journal International*, 236(1):688–699, Nov. 2023. doi: 10.1093/gji/ggad399.

Behm, M. and Snieder, R. Love waves from local traffic noise interferometry. *The Leading Edge*, 32(6):628–632, June 2013. doi: 10.1190/tle32060628.1.

Behm, M., Leahy, G. M., and Snieder, R. Retrieval of local surface wave velocities from traffic noise – an example from the La Barge basin (Wyoming). *Geophysical Prospecting*, 62(2): 223–243, Nov. 2013. doi: 10.1111/1365-2478.12080.

Brenguier, F., Boué, P., Ben-Zion, Y., Vernon, F., Johnson, C., Mordret, A., Coutant, O., Share, P., Beaucé, E., Hollis, D., and Lecocq, T. Train Traffic as a Powerful Noise Source for Monitoring Active Faults With Seismic Interferometry. *Geophysical Research Letters*, 46(16):9529–9536, Aug. 2019. doi: 10.1029/2019gl083438.

Brown, L., Davenport, K., Quiros, D., Han, L., Chen, C., and Hole, J. Aftershock Imaging with Dense Arrays (AIDA) following the August 23, 2011, Mw 5.8, Virginia Earthquake: Feasibility Demonstration and Preliminary Results. In *AGU Fall Meeting Abstracts*, page 14 –06, 2011.

Brown, L., Davenport, K., Quiros, D., Hole, J., Han, L., and Horowitz, F. Aftershock Imaging with Dense Arrays (AIDA): Results and lessons learned from the dense deployment of EarthScope portable instruments following the August 23, 2011, Mw 5.8, Virginia Earthquake. In *AGU Fall Meeting Abstracts*, volume 2021, page 51 –2462, 2012.

Chamarczuk, M., Malinowski, M., Draganov, D., Koivisto, E., Heinonen, S., and Rötsä, S. Reflection imaging of complex geology in a crystalline environment using virtual-source seismology: case study from the Kylylahti polymetallic mine, Finland. *Solid Earth*, 13(3):705–723, Mar. 2022. doi: 10.5194/se-13-705-2022.

Claerbout, J. F. Synthesis of a Layered Medium from its Acoustic Transmission Response. *GEOPHYSICS*, 33(2):264–269, Apr. 1968. doi: 10.1190/1.1439927.

Draganov, D., Wapenaar, K., and Thorbecke, J. *Seismic Interferometry: History and Present Status*. Society of Exploration Geophysicists, Jan. 2008. doi: 10.1190/1.9781560801924.

Ekström, G. Time domain analysis of Earth's long-period background seismic radiation. *Journal of Geophysical Research: Solid Earth*, 106(B11):26483–26493, Nov. 2001. doi: 10.1029/2000jb000086.

Halliday, D., Curtis, A., and Kragh, E. Seismic surface waves in a suburban environment: Active and passive interferometric methods. *The Leading Edge*, 27(2):210–218, Feb. 2008. doi: 10.1190/1.2840369.

Haubrich, R. A., Munk, W. H., and Snodgrass, F. E. Comparative spectra of microseisms and swell. *Bulletin of the Seismological Society of America*, 53(1):27–37, Jan. 1963. doi: 10.1785/bssa0530010027.

Holbrook, W. S., Fer, I., Schmitt, R. W., Lizarralde, D., Klymak, J. M., Helfrich, L. C., and Kubichek, R. Estimating oceanic turbulence dissipation from seismic images. *Journal of Atmospheric and Oceanic Technology*, 30, 2013. doi: 10.1175/JTECH-D-12-00140.1.

Liu, L., Liu, Y., Li, T., He, Y., Du, Y., and Luo, Y. Inversion of vehicle-induced signals based on seismic interferometry and recurrent neural networks. *GEOPHYSICS*, 86(3):Q37–Q45, Apr. 2021. doi: 10.1190/geo2020-0498.1.

Matsuoka, T., Shiraishi, K., Onishi, K., and Aizawa, T. Application of seismic interferometry to subsurface imaging (1). In *Proceedings of the 10th International Symposium on Recent Advanced in Exploration Geophysics (RAEG2006)*, page 35–38. Kyoto University Geophysical Society, 2006.

Meng, H., Ben-Zion, Y., and Johnson, C. W. Analysis of Seismic Signals Generated by Vehicle Traffic with Application to Derivation of Subsurface Q-Values. *Seismological Research Letters*, 92(4): 2354–2363, Feb. 2021. doi: 10.1785/0220200457.

Mi, B., Xia, J., Tian, G., Shi, Z., Xing, H., Chang, X., Xi, C., Liu, Y., Ning, L., Dai, T., Pang, J., Chen, X., Zhou, C., and Zhang, H. Near-surface imaging from traffic-induced surface waves with dense linear arrays: An application in the urban area of Hangzhou, China. *GEOPHYSICS*, 87(2):B145–B158, Feb. 2022. doi: 10.1190/geo2021-0184.1.

Miyazawa, M., Snieder, R., and Venkataraman, A. Application of seismic interferometry to extract P- and S-wave propagation and observation of shear-wave splitting from noise data at Cold Lake, Alberta, Canada. *GEOPHYSICS*, 73(4):D35–D40, July 2008. doi: 10.1190/1.2937172.

Nakata, N., Snieder, R., Larner, K., Tsuji, T., and Matsuoka, T. Shear-wave imaging from traffic noise using seismic interferometry by cross-coherence. In *SEG Technical Program Expanded Abstracts 2011*, page 1580–1585. Society of Exploration Geophysicists, Jan. 2011. doi: 10.1190/1.3627505.

Nakata, N., Chang, J. P., Lawrence, J. F., and Boué, P. Body wave extraction and tomography at Long Beach, California, with ambient-noise interferometry. *Journal of Geophysical Research: Solid Earth*, 120(2):1159–1173, Feb. 2015. doi: 10.1002/2015jb011870.

Quiros, D. Metadata for Raw Seismic Data for Traffic Interferometry experiment from Ithaca, NY, USA [dataset]. University of Cape Town, 2025a. doi: 10.25375/uct.28688210.v1.

Quiros, D. Raw Seismic Data for Traffic Interferometry Experiment from Ithaca, NY, USA [dataset]. University of Cape Town, 2025b. doi: 10.25375/uct.28687148.v1.

Quiros, D. A., Brown, L. D., and Kim, D. Seismic interferometry of railroad induced ground motions: body and surface wave imaging. *Geophysical Journal International*, 205(1):301–313, Feb. 2016. doi: 10.1093/gji/ggw033.

Riahi, N. and Gerstoft, P. The seismic traffic footprint: Tracking trains, aircraft, and cars seismically. *Geophysical Research Letters*, 42(8):2674–2681, Apr. 2015. doi: 10.1002/2015gl063558.

Roux, P., Sabra, K. G., Gerstoft, P., Kuperman, W. A., and Fehler, M. C. P-waves from cross-correlation of seismic noise. *Geophysical Research Letters*, 32(19), Oct. 2005. doi: 10.1029/2005gl023803.

Ruigrok, E., Campman, X., Draganov, D., and Wapenaar, K. High-

resolution lithospheric imaging with seismic interferometry. *Geophysical Journal International*, 183(1):339–357, Aug. 2010. doi: 10.1111/j.1365-246x.2010.04724.x.

Ryberg, T. Body wave observations from cross-correlations of ambient seismic noise: A case study from the Karoo, RSA. *Geophysical Research Letters*, 38(13), July 2011. doi: 10.1029/2011gl047665.

Schuster, G. T., Yu, J., Sheng, J., and Rickett, J. Interferometric/daylight seismic imaging. *Geophysical Journal International*, 157(2): 838–852, May 2004. doi: 10.1111/j.1365-246x.2004.02251.x.

Shapiro, N. M., Campillo, M., Stehly, L., and Ritzwoller, M. H. High-Resolution Surface-Wave Tomography from Ambient Seismic Noise. *Science*, 307(5715):1615–1618, Mar. 2005. doi: 10.1126/science.1108339.

Shiraishi, K., Tanaka, M., Onishi, K., Matsuoka, T., and Yamaguchi, S. Application of Seismic Interferometry to Subsurface Imaging (2). In *The 10th International Symposium on Recent Advances in Exploration Geophysics (RAEG 2006)*. European Association of Geoscientists & Engineers, 2006. doi: 10.3997/2352-8265.20140076.

Snieder, R. Extracting the Green's function from the correlation of coda waves: A derivation based on stationary phase. *Physical Review E*, 69(4), Apr. 2004. doi: 10.1103/physreve.69.046610.

Spangler, M. A. and Nowack, R. L. Seismic Interferometry Applied to Wind Farm and Other Anthropogenic Noise Sources. *Seismological Research Letters*, 94(1):123–139, Aug. 2022. doi: 10.1785/0220220201.

Suhey, J., Katz, Z., Zhang, M., Ferris, A., Pritchard, M., Salerno, J., Hubbard, P., and Gustafson, J. Analysis of Cornell University's Seismic Networks for the Earth Source Heat Initiative. In *Cornell Earth Source Heat Project: Technical Reports and Datasets*. 2021. https://hdl.handle.net/1813/103518.

Tamulonis, K. L., Jordan, T. E., and Slater, B. Carbon dioxide storage potential for the Queenston Formation near the AES Cayuga coal-fired power plant in Tompkins County, New York. *Environmental Geosciences*, 18(1):1–17, Mar. 2011. doi: 10.1306/eg.05191010005.

The ObsPy Development Team. ObsPy 1.4.1 [software]. Zenodo, 2024. doi: 10.5281/zenodo.11093256.

Tian, D., Uieda, L., Leong, W. J., Fröhlich, Y., Schlitzer, W., Grund, M., Jones, M., Toney, L., Yao, J., Tong, J.-H., Magen, Y., Materna, K., Belem, A., Newton, T., Anant, A., Ziebarth, M., Quinn, J., and Wessel, P. PyGMT: A Python interface for the Generic Mapping Tools [software]. Zenodo, 2025. doi: 10.5281/zenodo.15071586.

Toksöz, M. N. and Lacoss, R. T. Microseisms: Mode Structure and Sources. *Science*, 159(3817):872–873, Feb. 1968. doi: 10.1126/science.159.3817.872.

Wapenaar, K. Synthesis of an inhomogeneous medium from its acoustic transmission response. *GEOPHYSICS*, 68(5):1756–1759, Sept. 2003. doi: 10.1190/1.1620649.

Wapenaar, K. Retrieving the Elastodynamic Green's Function of an Arbitrary Inhomogeneous Medium by Cross Correlation. *Physical Review Letters*, 93(25), Dec. 2004. doi: 10.1103/physrevlett.93.254301.

Wapenaar, K. and Fokkema, J. Green's function representations for seismic interferometry. *GEOPHYSICS*, 71(4):SI33–SI46, July 2006. doi: 10.1190/1.2213955.

Wapenaar, K., Thorbecke, J., and Draganov, D. Relations between reflection and transmission responses of three-dimensional inhomogeneous media. *Geophysical Journal International*, 156 (2):179–194, Feb. 2004. doi: 10.1111/j.1365-246x.2003.02152.x.